Applied Mathematical Modelling 116 (2023) 236–253

Contents lists available at ScienceDirect

Applied Mathematical Modelling

journal homepage: www.elsevier.com/locate/apm

Efficient self-propelled locomotion by an elastically supported rigid foil actuated by a torque

P.E. Lopez-Tello, R. Fernandez-Feria*, E. Sanmiguel-Rojas

Fluid Mechanics Group, Universidad de Málaga, Dr Ortiz Ramos s/n, Málaga 29071, Spain

ARTICLE INFO

Article history:
Received 12 July 2022
Revised 14 October 2022
Accepted 9 November 2022
Available online 19 November 2022

Keywords:
Propulsion
Fluid-structure interaction
Flapping foil
Analytical model

ABSTRACT

A new theoretical model is presented for an aquatic vehicle self-propelled by a rigid foil undergoing pitching oscillations generated by a torque of small amplitude applied at an arbitrary pivot axis at which the foil is elastically supported to allow for passive heaving motion. The model is based on 2D linear potential-flow theory coupled with the self-propelled dynamics of the semi-passive flapping foil elastically mounted on the vehicle hull through translational and torsional springs and dampers. It is governed by just three ordinary differential equations, whose numerical solutions are assessed with full viscous numerical simulations of the self-propelled foil. Analytical approximate solutions for the combined effect of all the relevant non-dimensional parameters on the swimming velocity and efficiency are also obtained by taking advantage of the small-amplitude of the applied torque. Thus, simple power laws for the velocity and efficiency dependencies on Lighthill number and torque intensity are obtained. It is found that the swimming velocity and transport efficiency can be greatly enhanced by selecting appropriately the non-dimensional constants of the translational and torsional springs, which are mapped for typical values of the remaining parameters in aquatic locomotion. These resonant values serve to select optimal frequencies of the forcing torque for given structural and geometric parameters. Thus, the present model and analysis provide a useful guide for the design of an efficient flapping-foil underwater vehicle.

1. Introduction

Several aquatic propulsion technologies based on flapping foils, mostly bioinspired on efficient swimming animals, have been developed in the past few decades [1–4]. In addition to be able to reach sufficiently high propulsion efficiencies, these flapping propellers may have some other advantages in relation to traditional rotating propellers depending on how the flapping foils are configured, including high maneuverability, easy control, low-frequency and less cavitation problems, among others. Of the many configurations that have been proposed and studied, we consider here a particular one consisting of a rigid foil with a pitching motion generated by a given torque, but with torsional spring and damper to allow the pitching motion to adapt passively to the forcing torque, and with a fully passive heaving motion of the foil elastically

* Corresponding author.
E-mail addresses: pe.lopeztello@gmail.com (P.E. Lopez-Tello), ramon.fernandez@uma.es (R. Fernandez-Feria), enrique.sanmiguel@uma.es (E. Sanmiguel-Rojas).

https://doi.org/10.1016/j.apm.2022.11.007

mounted to translational spring and damper. In relation to fully constrained configurations of rigid foils, this one allows for the possibility of resonant modes of the pitching and heaving motions that, as we shall see, may greatly enhance the thrust force and, therefore, the swimming velocity and the propulsive efficiency.

It is widely known that a semi-passive flapping foil configuration consisting of a forced pitching foil with passive heave may enhance their performance by resonant phenomena in both propulsion [5–7] and energy harvesting [8–12] systems. However, to our knowledge, the self-propulsion performance of a vehicle propelled by such a flapping-foil configuration, where its forward velocity is generated by the thrust force produced by the elastically mounted flapping foil, instead of just considering its propulsive performance in a uniform current, has not been analyzed. This study involves the complex fluid-structure interaction of the rigid foil elastically mounted to translational springs and dampers anchored to the vehicle hull, practically infeasible to solve using full numerical simulations. For that reason we use here a model based on linear potential-flow coupled with the dynamics of the elastically mounted rigid foil to the vehicle. The model is validated by comparing its performance with full numerical simulations of the viscous-flow in the limit of large translational spring constant, so that the heaving motion of the self-propelled foil is inhibited [13].

The self-propulsion performance of isolated rigid foils with prescribed pitching and/or heaving motion has been studied theoretically, experimentally and numerically [14–18]. In the pioneering work by Alben and Shelley [14] it was shown numerically that a foil undergoing a vertical heaving motion within a viscous fluid may spontaneously develop, for sufficiently large frequency Reynolds number, a unidirectional horizontal locomotion as an attracting state for an initial nonlocomoting foil. In their interesting theoretical study on a self-propelled foil with prescribed pitching motion, Sanchez-Rodriguez et al. [15] also used, like in the present work, analytical results from the linear potential-flow theory to model the lift and thrust forces that the fluid exerts on the foil, but with a different model for the thrust. Additionally, here we consider the more realistic situation of an elastically mounted foil whose pitching motion is generated by a given torque applied at an arbitrary pivot axis, instead of being prescribed, and coupled to a passive heaving motion, thus taking advantage of the resonances arising in the elastically mounted system to enhance the propulsion of the vehicle where this propeller is anchored.

2. Formulation of the problem

We consider an underwater vehicle like, for instance, that sketched in Fig. 1(a), self propelled by a thin rigid hydrofoil through pitching and passive heaving motions. The foil has a large aspect ratio, so that the flow and the fluid-foil interaction are assumed two-dimensional (2D). It is actuated at a pivot point located at $\tilde{x}' = \tilde{a}$ by a sinusoidal torque per unit span $M_i(t)$, where $\tilde{x}'$ is the coordinate along the foil centerline from the mid-chord (see Fig. 1(b); a tilde $\tilde{}$ over a symbol denotes a dimensional quantity, and it is only used when the same symbol without the tilde will be employed later for its dimensionless counterpart). The foil is elastically mounted to translational and torsional springs and dampers at the pivot point, with dimensional constants $\tilde{k}_h$ and $\tilde{k}_\alpha$ for the springs, and $\tilde{b}_h$ and $\tilde{b}_\alpha$ for the dampers, respectively. The corresponding force (along the transversal coordinate $\tilde{z}$) and torque exerted by these springs and dampers at the pivot point are denoted in Fig. 1(a) by L_o and M_o, respectively, both per unit span.

In what follows all magnitudes are made dimensionless with the semi-chord length $c/2$, the fluid density ρ and the frequency ω of the input torque, which in dimensionless form is given by

$$\hat{C}_{M_i} := \frac{8M_i}{\pi \rho c^4 \omega^2} = \epsilon \sin t, \tag{1}$$

where ϵ is the (known) non-dimensional torque intensity, which will be assumed small in the model described in Sections 3 and 4. This torque induces a pitching motion $\alpha(t)$ about $x' = a$, where the dimensionless pivot point location may vary from $a = -1$ (leading edge) to $a = 1$ (trailing edge). Due to the fluid-structure interaction (FSI) and to the action of the translational and torsional springs and dampers, the foil also undergoes a (passive) heaving motion along the z direction whose dimensionless amplitude will be denoted by $h(t)$. Both $h(t)$ and $\alpha(t)$ are unknowns. Additionally, the hydrofoil moves together with the vehicle it propels in the negative x direction at a dimensionless velocity $u(t)$, also unknown, so that in the vehicle reference frame (x, z) the free-stream velocity towards the foil is $u(t)$ (see Fig. 1(b)). Remember that this velocity is scaled with $\omega c/2$, which means that $u(t)$ is actually the inverse of the reduced frequency $k(t)$ commonly used in unsteady aerodynamics [19], which now depends on time,

$$u(t) := \frac{2\tilde{u}(t)}{\omega c} = \frac{1}{k(t)}\,. \tag{2}$$

The dynamics of the rigid foil is governed by the following two non-dimensional equations (momentum in the z direction and moment around the pivot axis, respectively):

$$R\Big[\dot{v} + (a - x_0)\big(\ddot{\alpha}\cos\alpha - \dot{\alpha}^2 \sin\alpha\big)\Big] = \hat{C}_L + \hat{C}_{L_i} - \hat{C}_{L_o}\,, \qquad v := \dot{h}\,, \tag{3}$$

$$R[(x_0 - a)\dot{v}\cos\alpha - I_a\ddot{\alpha}] = 2(\hat{C}_M + \hat{C}_{M_i} - \hat{C}_{M_o})\,, \tag{4}$$

with

$$\hat{C}_{L_o} = k_h h + b_h v\,, \quad \hat{C}_{M_o} = -k_\alpha \alpha - b_\alpha \dot{\alpha}\,, \tag{5}$$

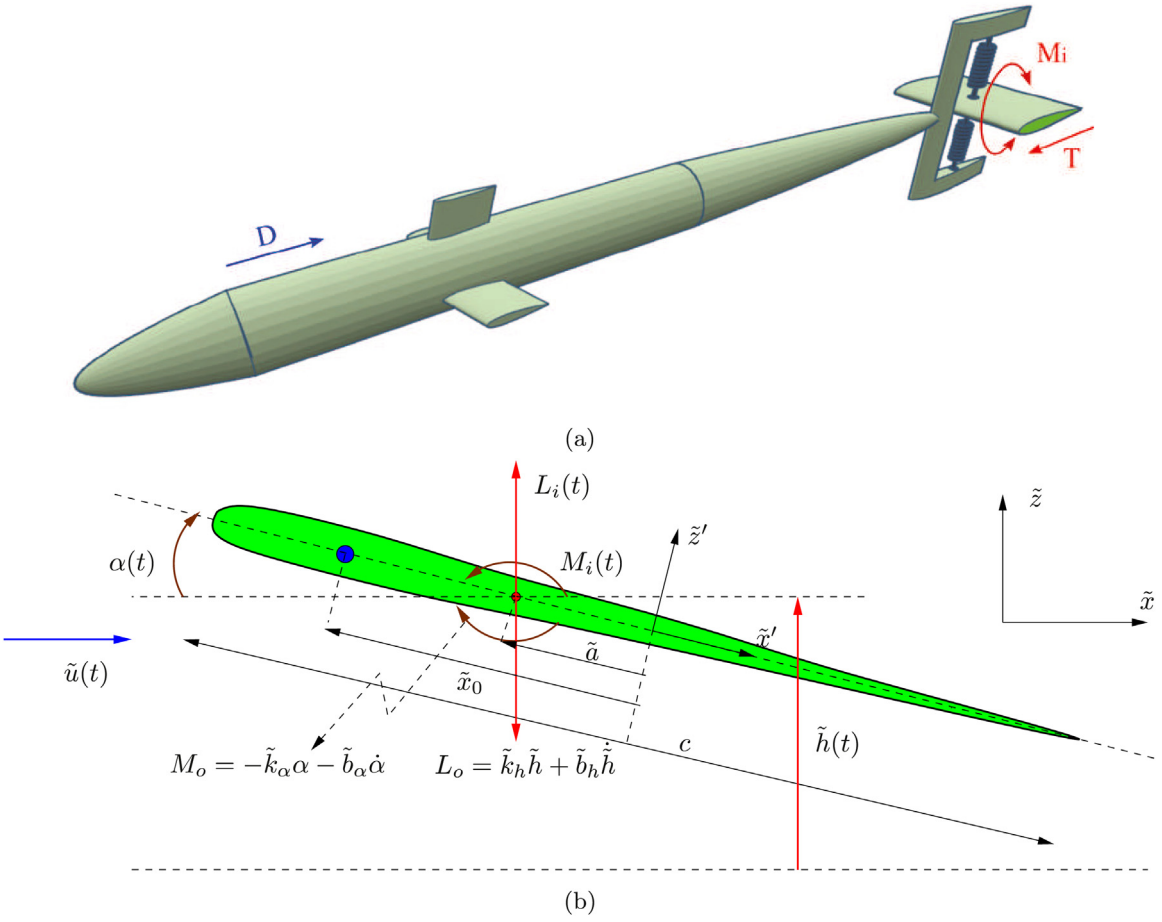

Fig. 1. Sketch of a vehicle (a) self-propelled by an elastically supported foil (b). Dimensional quantities (see main text).

where each dot denotes a derivative with respect to the dimensionless time t (scaled with ω) and v is the dimensionless heave velocity. In these equations, $\hat{C}_L$ and $\hat{C}_M$ are the non-dimensional force component in the z direction and the non-dimensional moment, respectively, that the fluid exerts on the foil per unit span,

$$\hat{C}_L := \frac{8L}{\pi\rho c^3\omega^2}\,, \quad \hat{C}_M := \frac{8M}{\pi\rho c^4\omega^2}\,. \tag{6}$$

We have also included in Eqs. (3)-(4) an input force in the z direction $\hat{C}_{L_i}(t)$ for completeness (see also Fig. 1(b)), though it will be set to zero in the reported results. The 'hat' $\hat{}$ on all these coefficients is to remark that they are not the usual lift and moment coefficients, C_L and C_M, scaled with $\frac{1}{2}\rho u^2 c$ and $\frac{1}{2}\rho u^2 c^2$, respectively; they are related to each other through

$$C_L := \frac{2L}{\rho\tilde{u}^2 c} = \frac{\pi\hat{C}_L}{u^2}\,, \quad C_M := \frac{2M}{\rho\tilde{u}^2 c^2} = \frac{\pi\hat{C}_M}{u^2}\,, \tag{7}$$

and similarly for $\hat{C}_{M_i}$ and $\hat{C}_{L_i}$. In addition to the pivot point location a, the non-dimensional parameters appearing in Eqs. (3)-(5) are the mass ratio R, the center of mass x_0, the moment of inertia about the pivot point I_a, the translational and torsional spring stiffnesses k_h and k_α, and the translational and torsional damper constants b_h and b_α. Note that $R(x_0 - a)$ is the non-dimensional static moment about $x = a$. In terms of the foil's density and thickness distributions, $\rho_s(\tilde{x}')$ and $\gamma(\tilde{x}')$, respectively, the first three ones are defined as

$$R = \frac{4m}{\pi\rho c^2}\,, \quad m = \int_{-c/2}^{c/2}\rho_s\gamma\, d\tilde{x}'\,, \tag{8}$$

$$x_0 = \frac{1}{2}\int_{-1}^{1} x'\mathcal{M}dx'\,, \quad I_a = \frac{1}{2}\int_{-1}^{1}(x'-a)^2\mathcal{M}dx'\,, \qquad \mathcal{M} := \frac{\rho_s\gamma c}{m}\,, \tag{9}$$

where m is the mass of the hydrofoil per unit span. If the density ρ_s and the thickness γ were constants, $\mathcal{M} = 1$, so that the center of mass would be at the mid-chord, $x_0 = 0$, and

$$I_a = a^2 + \frac{1}{3}\,. \tag{10}$$

Also note that we do not assume that the pivot point location coincides with the center of mass. It remains to define the spring and damper constants, related to their dimensional counterparts (per unit span) through

$$k_h = \frac{4\tilde{k}_h}{\pi\rho c^2\omega^2}\,, \quad b_h = \frac{4\tilde{b}_h}{\pi\rho c^2\omega}\,, \quad k_\alpha = \frac{8\tilde{k}_\alpha}{\pi\rho c^4\omega^2}\,, \quad b_\alpha = \frac{8\tilde{b}_\alpha}{\pi\rho c^4\omega}\,. \tag{11}$$

In relation to the equation of motion along the x direction, we use Newton's second law applied to the vehicle center of mass, to write, in dimensionless form,

$$R'\dot{u} = \hat{C}_T - Li\,u^2\,. \tag{12}$$

In this equation,

$$\hat{C}_T := \frac{8T}{\pi\rho c^3\omega^2} = \frac{u^2 C_T}{\pi} \tag{13}$$

is the non-dimensional thrust force that the fluid exerts on the hydrofoil and propels the vehicle in the $-x$ direction, with T the dimensional thrust force per unit span, and $Li\,u^2$ the vehicle's non-dimensional drag force written in terms of the Lighthill number Li, related to the drag coefficient C_D by

$$Li := \frac{A_w}{\pi cs}C_D\,, \quad \text{with} \quad C_D := \frac{2D}{\rho\tilde{u}^2 A_w}\,, \tag{14}$$

where D is the drag force (see Fig. 1(a)), A_w is a characteristic surface of the vehicle and s is the foil's span length. Note that u and $\hat{C}_T$ are assumed positive when pointing in the direction of negative x, while the drag force is positive in the opposite direction. For simplicity we shall assume that C_D is constant in the relevant range of Reynolds numbers for underwater propulsion [20,21]. Finally,

$$R' = \frac{4m'}{\pi\rho c^2 s} \tag{15}$$

is the dimensionless mass ratio of the underwater vehicle, with m' its total mass [contrary to m in (8), which has units of mass per unit span of the foil, m' has units of mass]. We shall not consider the vehicle's vertical motion due to the action of gravity, which in any case can be minimized using a neutrally buoyant vehicle.

Eqs. (3), (4) and (12) constitute a set of three ordinary differential equations (ODEs) for $h(t)$ [or $v(t)$], $\alpha(t)$ and $u(t)$ that can be solved for the given torque (1) if the coefficients $\hat{C}_L(t)$, $\hat{C}_M(t)$ and $\hat{C}_T(t)$ coming from the FSI are known in terms of h, α and u (see §3 below). But before that, it is convenient to define some relevant quantities to characterize the vehicle's self-propulsion.

Once Eqs. (3), (4) and (12) are solved for a given set of initial conditions, the solution will eventually reach a final *permanent* state consisting of an oscillatory periodic motion around a mean, or time-averaged, value of each variable. These mean quantities will be denoted by an over-bar, and, except otherwise specified, will be computed by averaging over a cycle of the forcing torque,

$$\overline{X} = \frac{1}{2\pi}\int_t^{t+2\pi} X(t')dt'\,, \tag{16}$$

for any magnitude $X(t)$ and with t sufficiently large. Of particular relevance is the mean swimming speed $U = \overline{u}$, or mean value of u as $t \to \infty$, which in some circumstances is of interest to maximize in terms of the different parameters governing the problem. Notice that once a constant swimming velocity U has been reached, the time-average of the left hand side of Eq. (12) vanishes, and so does the mean of the right hand side. Thus, the mean thrust generated by the flapping hydrofoil becomes equal to the mean drag of the whole cruising vehicle: $\overline{\hat{C}}_T = Li\,\overline{u^2} > 0$ for $t \to \infty$.

Alternatively, one may be interested in maximizing the propulsive (Froude) efficiency. To compute it, one has to obtain previously the input power needed to generate the oscillatory motion of the foil. The (instantaneous) input power P is defined as the product of the heave velocity by the input lift plus the product of the angular velocity times the input torque. In dimensionless form, scaled with $\pi\rho c^4\omega^3/16$,

$$\hat{C}_P := \frac{16P}{\pi\rho c^4\omega^3} = \dot{h}\hat{C}_{L_i} - 2\dot{\alpha}\hat{C}_{M_i}\,. \tag{17}$$

(Note that the minus sign comes from the different sign convention for the pitch angle and the input torque; see Fig. 1.) In the present work we assume $\hat{C}_{L_i} = 0$, so that the heaving motion, if any, is passive, and all the input power is associated to the input torque. On the other hand, the (instantaneous) propulsive power coefficient is the product of $\tilde{u}$ times the thrust

force that generates this speed scaled with the same characteristic power used above; i.e., $u\hat{C}_T$. The propulsive efficiency is the ratio of these two quantities when time-averaged,

$$\eta = \frac{\overline{u\hat{C}_T}}{\bar{\hat{C}}_P} = \frac{R'\,\overline{u\dot{u}} + Li\,\overline{u^3}}{\bar{\hat{C}}_P} \simeq \frac{Li\,\overline{u^3}}{\bar{\hat{C}}_P}\,, \tag{18}$$

where Eq. (12) has been used. The last expression after '$\simeq$' comes from the fact that once the final oscillatory state has been reached, u becomes an almost harmonic function of time and $\overline{u\dot{u}} \simeq 0$. From this expression it results that, for given powering torque and vehicle's drag (Li), maximizing the dimensionless swimming velocity U is equivalent to maximizing η. Note, however, that the swimming velocity is scaled with the selected forcing frequency ω.

It is known that maximum propulsive efficiency is usually reached in a narrow range of the Strouhal number [22], which is defined as

$$St = \frac{\omega\tilde{A}}{2\pi\tilde{U}} = \frac{A}{2\pi U}\,, \tag{19}$$

where $\tilde{A}$ is the beat amplitude, taken as the maximum peak-to-peak flapping foil amplitude (A is its dimensionless counterpart). Thus, sometimes it is more interesting to characterize the cruising velocity U in terms of St, usually in combination with the corresponding Reynolds number, $Re = \tilde{U}c/\nu$, [23] where ν is the kinematic viscosity.

Finally, for cruising, it is sometimes preferable the use of the cost of transport instead to the Froude efficiency as a measure of the *self*-propulsion efficiency [18,24]. It is defined as the energy consumption per unit distance travelled by the vehicle:

$$\widetilde{CoT} = \frac{\bar{P}}{\tilde{U}} = \frac{\pi\rho c^3 s\,\omega^2}{8}\,CoT\,, \qquad CoT = \frac{\bar{\hat{C}}_P}{U}\,, \tag{20}$$

where CoT is a dimensionless cost of transport that will be used in the reported results. Some authors use the non-dimensional cost of transport $\bar{P}/(W\tilde{U})$, where W is the weight of the vehicle, but we believe that the above CoT is more consistent with the present non-dimensionalization. In any case, the results would be scaled by just a constant factor.

3. Linearized model

If the torque intensity ϵ is small enough, one may assume that the pitch and heave amplitudes are also small, $|\alpha| \ll 1$ and $|h| \ll 1$, so that one may use the expressions of $\hat{C}_L(t)$, $\hat{C}_M(t)$ and $\hat{C}_T(t)$ from the linear potential flow theory for a harmonic foil motion, but written in a general form in terms of α, h and u and their temporal derivatives. In particular, we use Theodorsen's expressions for the lift and moment coefficient [19], modified by [25] with additional terms proportional to $\dot{u}$ to account for the pulsating stream, and with Theodorsen's function appearing in the circulatory terms evaluated at variable $k(t) = 1/u(t)$. In the present notation,

$$\hat{C}_L(t) = -\dot{v} - a\ddot{\alpha} + u\dot{\alpha} + \dot{u}\alpha + \mathrm{Re}[\mathcal{C}(k)]u\Gamma_0(t)\,, \tag{21}$$

$$\hat{C}_M(t) = \frac{1}{2}\left[a\dot{v} + \left(a^2 + \frac{1}{8}\right)\ddot{\alpha} + \left(\frac{1}{2} - a\right)u\dot{\alpha} - a\dot{u}\alpha\right] - \frac{1}{2}\left(\frac{1}{2} + a\right)\mathrm{Re}[\mathcal{C}(k)]u\Gamma_0(t)\,, \tag{22}$$

$$\Gamma_0(t) = -2\left[v + \left(a - \frac{1}{2}\right)\dot{\alpha} - u\alpha\right], \tag{23}$$

where

$$\mathcal{C}(k) = \frac{H_1^{(2)}(k)}{iH_0^{(2)}(k) + H_1^{(2)}(k)} = \mathcal{F}(k) + i\mathcal{G}(k) \tag{24}$$

is Theodorsen's function and Re means real part. These force and moment, which have been widely validated against experimental data for pitching and heaving rigid foils even for not so small amplitude of the oscillations [26,27], are used in the linearized form of Eqs. (3) and (4):

$$R[\dot{v} + (a - x_0)\ddot{\alpha}] = \hat{C}_L + \hat{C}_{L_i} - \hat{C}_{L_o}\,, \qquad \dot{h} = v\,, \tag{25}$$

$$R[(x_0 - a)\dot{v} - I_a\ddot{\alpha}] = 2(\hat{C}_M + \hat{C}_{M_i} - \hat{C}_{M_o})\,, \tag{26}$$

where now $x' \simeq x$ and $z' \simeq z$.

As for the thrust coefficient, we shall use in Eq. (12) the result from the linearized vortical impulse theory [28], which has been validated against experimental data for small amplitude of the oscillations and sufficiently large Reynolds numbers, both for pitching and heaving foils in a uniform flow [28–31] and for self-propelled pitching foils [13]. In the present notation it can be written as

$$\hat{C}_T = -\alpha\hat{C}_L + \dot{\alpha}[v + a\dot{\alpha} - u\alpha] + \Gamma_0\left\{\mathrm{Re}\left[\frac{2i\mathcal{C}_1(k)}{\pi}\right][-v + 2\alpha u + (1 - a)\dot{\alpha}] - \mathrm{Re}[\mathcal{C}(k)]u\alpha\right\}, \tag{27}$$

where

$$\mathcal{C}_1(k) = \frac{\frac{1}{k}e^{-ik}}{iH_0^{(2)}(k) + H_1^{(2)}(k)} = \mathcal{F}_1(k) + i\mathcal{G}_1(k)\,. \tag{28}$$

The resulting system of ODEs (25), (26) and (12) is solved numerically for $h(t)$, $\alpha(t)$ and $u(t)$ as described in Section 6 below.

The present self-propulsion model is more general than the one considered by Sanchez-Rodriguez et al. [15], where a prescribed pitching kinematics is used, $\alpha(t) = \alpha_0 \sin t$ in the present notation, instead of the more realistic torque (1) used here. Consequently, we need the additional moment Eq. (26) which is not considered in [15]. This is also physically relevant because we can compute the input power, and therefore, the propulsive efficiency and the cost of transport, which cannot be obtained with the simpler model by Sanchez-Rodriguez et al. [15]. Therefore we can select the sets of parameters that produce the optimal efficiency or the optimal cost of transport. Additional translational and torsional springs and dampers are also used here, which enriches the model and whose characteristics may be varied to improve the propulsion performance due to resonance between passive and forced motions [32]. Further, the pivot axis location $x = a$ is set here independently of the center of mass of the foil $x = x_0$, so that one may explore its effect on the propulsion performance separately. Finally, we use expression (27) for the thrust, which, though yielding practically the same results as Garrick's [33] thrust used in [15] at low reduced frequencies, has proven to agree better with experimental data in a wider range of parameters [28,30,31]. The differences are particularly relevant for high reduced frequencies, corresponding to the small velocity limit considered in next section's asymptotic analysis (remember that $u = 1/k$).

4. Approximate analytical solution from two-scales perturbation method

Alternatively to the numerical solution of the model Eqs. (25), (26) and (12), one may take advantage of the small torque intensity ϵ to obtain an analytical approximation for $h(t)$, $\alpha(t)$ and $u(t)$ using perturbation methods. In particular, from the structure of the equations one might assume two timescales: t, associated to period of the oscillations, and

$$\tau = B\epsilon^b t\,, \tag{29}$$

associated to the slower variations of the mean values, where the constants B and b will be determined from the scaling of the different terms in Eq. (12). Thus, the time derivatives are approximated by

$$\frac{d}{dt} = \frac{\partial}{\partial t} + B\epsilon^b \frac{\partial}{\partial \tau}\,. \tag{30}$$

Assuming that, according to (25)-(26), the lowest order amplitude of the pitching and heaving oscillations is of the same order ϵ as the forcing torque $\hat{C}_{M_i}$, the asymptotic expansions for h and α with the two timescales can be written as

$$h(t,\tau) \sim \epsilon h_1(t,\tau) + \epsilon^2 h_2(t,\tau) + \ldots, \quad \alpha(t,\tau) \sim \epsilon\alpha_1(t,\tau) + \epsilon^2\alpha_2(t,\tau) + \ldots\,. \tag{31}$$

As we shall see, only the next terms in these expansions depend on the expansion of u if, as shown below, $u \ll \epsilon$. In general, we can write the expansion for u as

$$u(t,\tau) \sim \epsilon^{n_1} u_1(t,\tau) + \epsilon^{n_2} u_2(t,\tau) + \ldots, \tag{32}$$

with $1 < n_1 < n_2 < \ldots$ to be determined.

To perform the expansions for the force and moment coefficients we take into account that $k = u^{-1} \gg 1$, so that one may use the large-k approximation of the functions (24) and (28) [30] to write

$$\mathrm{Re}[C(k)] = \frac{1}{2} + O(k^{-2})\,, \quad \mathrm{Re}\left[\frac{2i\mathcal{C}_1(k)}{\pi}\right] = \frac{1}{(4\pi k)^{1/2}} + O(k^{-3/2})\,. \tag{33}$$

Since it will turn out that both b and n_1 are larger than unity, the two leading terms of $\hat{C}_L$ and $\hat{C}_M$ are

$$\hat{C}_L \sim -\epsilon\left(\frac{\partial^2 h_1}{\partial t^2} + a\frac{\partial^2 \alpha_1}{\partial t^2}\right) - \epsilon^2\left(\frac{\partial^2 h_2}{\partial t^2} + a\frac{\partial^2 \alpha_2}{\partial t^2}\right) + O(\epsilon^{1+b}, \epsilon^{1+n_1})\,, \tag{34}$$

$$\hat{C}_M \sim \epsilon\left[a\frac{\partial^2 h_1}{\partial t^2} + \left(a^2 + \frac{1}{8}\right)\frac{\partial^2 \alpha_1}{\partial t^2}\right] + \epsilon^2\left[a\frac{\partial h_2^2}{\partial t^2} + \left(a^2 + \frac{1}{8}\right)\frac{\partial \alpha_2^2}{\partial t^2}\right] + O(\epsilon^{1+b}, \epsilon^{1+n_1})\,. \tag{35}$$

After substituting into (25) and (26), one gets two pairs of equations for the two leading orders of h and α, which are independent of u. At the lowest order (ϵ) these equations are

$$O(\epsilon): \quad \begin{cases} \left(R+1\right)\dfrac{\partial^2 h_1}{\partial t^2} + \left[R(a-x_0)+a\right]\dfrac{\partial^2 \alpha_1}{\partial t^2} + b_h\dfrac{\partial h_1}{\partial t} + k_h h_1 = 0, \\ \left[R(x_0-a)-a\right]\dfrac{\partial^2 h_1}{\partial t^2} - \left[RI_a + \left(a^2+\dfrac{1}{8}\right)\right]\dfrac{\partial^2 \alpha_1}{\partial t^2} - 2b_\alpha\dfrac{\partial \alpha_1}{\partial t} - 2k_\alpha\alpha_1 = 2\sin t. \end{cases} \tag{36}$$

The solution to this system of two linear equations for h_1 and α_1 contains transient terms of the form $e^{\lambda_1 t}$ that decay very fast to zero from any initial condition provided that the real part of the eigenvalues λ_1 of the following determinant are all negative:

$$\begin{vmatrix} (R+1)\lambda_1^2 + b_h\lambda_1 + k_h & (a+R(a-x_0))\lambda_1^2 \\ (a+R(a-x_0))\lambda_1^2 & (RI_a + a^2 + 1/8)\lambda_1^2 + 2b_\alpha\lambda_1 + 2k_\alpha \end{vmatrix} = 0\,. \tag{37}$$

Only these stable solutions with $\mathrm{Re}(\lambda_1) < 0$ will be considered, which, for $x_0 = 0$, covers all the values of the mass ratio R if the pivot point is located upstream of the foil's mid-chord, $-1 \le a \le 0$ (see Appendix A). For $b_h = b_\alpha = 0$ (no dampers) the system is neutrally stable; i.e., $\mathrm{Re}(\lambda_1) = 0$.

Thus, discarding unstable solutions with $\mathrm{Re}(\lambda_1) > 0$, we only write the permanent, or particular, solution of Eqs. (36) associated to the forcing torque (term $2\sin t$ on the right hand side), which can be written as

$$h_1 = H_1 \sin(t+\phi_{h1})\,, \qquad \alpha_1 = A_1 \sin(t+\phi_{a1})\,, \tag{38}$$

where the complex constants

$$\mathcal{H}_1 \equiv H_1 e^{i\phi_{h1}} \quad \text{and} \quad \mathcal{A}_1 \equiv A_1 e^{i\phi_{a1}} \tag{39}$$

satisfy the linear system of equations

$$\mathbf{A}\cdot\begin{pmatrix}\mathcal{H}_1\\ \mathcal{A}_1\end{pmatrix} \equiv \begin{pmatrix} -(R+1) + b_h i + k_h & -(a+R(a-x_0)) \\ a+R(a-x_0) & RI_a + a^2 + 1/8 - 2b_\alpha i - 2k_\alpha \end{pmatrix}\cdot\begin{pmatrix}\mathcal{H}_1\\ \mathcal{A}_1\end{pmatrix} = \begin{pmatrix}0\\ 2\end{pmatrix}. \tag{40}$$

Of particular interest are the values of the spring constants k_h and k_α that maximize the heaving and pitching amplitudes, since the thrust force and, consequently, the swimming velocity U will be enhanced (see below). These values, denoted here by k_{hr} and $k_{\alpha r}$, are obtained by minimizing $|\det(\mathbf{A})|$, where $\mathbf{A}$ is the 2×2 matrix in (40), and physically correspond to particular resonant frequencies for given dimensional constants $\tilde{k}_h$ and $\tilde{k}_\alpha$ according to the non-dimensionalization (11). A good approximation for the resonant value of k_h when the damping constants b_h and b_α are small is the value of k_h for which $|\det(\mathbf{A})|$ actually vanishes when $b_h = b_\alpha = 0$; i.e.,

$$k_{hr0} = 1 + R - \frac{[a+R(a-x_0)]^2}{RI_a + a^2 + 1/8 - 2k_\alpha}\,. \tag{41}$$

Note that $k_{hr0} \to \infty$ for

$$k_\alpha = \frac{1}{2}\left(RI_a + a^2 + \frac{1}{8}\right) \equiv k_{\alpha\infty}\,. \tag{42}$$

It is interesting to remark that, with the present lowest order solution, the optimal propulsion conditions might be approximately predicted by just minimizing a rather simple algebraic expression such as $|\det(\mathbf{A})|$. This will be done in Section 5 below, considering not only the maximum of the time-averaged swimming velocity, but also the maximum efficiency and the minimum cost of transport.

Similarly, one may obtain the solution for the next order (ϵ^2) of both α and h, which is also independent of the swimming velocity u, but it will not be given here because we are only interested in the lowest order solution.

Although the solution for the heaving and pitching motions is independent of the swimming velocity up to order ϵ^2, u depends strongly on both, h and α, even at its lowest order through $\hat{C}_T$ in Eq. (12). Actually, the leading orders of the expansion for $\hat{C}_T$ can be written as

$$\hat{C}_T \sim \epsilon^2\left[\alpha_1\frac{\partial^2 h_1}{\partial t^2} + a\alpha_1\frac{\partial^2\alpha_1}{\partial t^2} + \frac{\partial\alpha_1}{\partial t}\frac{\partial h_1}{\partial t} + a\left(\frac{\partial\alpha_1}{\partial t}\right)^2\right]$$
$$+\epsilon^{2+n_1/2}\frac{u_1^{1/2}}{\sqrt{\pi}}\left[\left(\frac{\partial h_1}{\partial t}\right)^2 + \left(2a-\frac{3}{2}\right)\frac{\partial\alpha_1}{\partial t}\frac{\partial h_1}{\partial t} + \left(a-\frac{1}{2}\right)(a-1)\left(\frac{\partial\alpha_1}{\partial t}\right)^2\right] + \dots\,. \tag{43}$$

After substituting (38) into (43) and using the expansion (32), the leading order terms in Eq. (12) are

$$R'\left(\frac{\partial}{\partial t} + B\epsilon^b\frac{\partial}{\partial\tau}\right)(\epsilon^{n_1}u_1 + \epsilon^{n_2}u_2 + \epsilon^{n_3}u_3 + \dots) = \epsilon^2 A_1\left\{H_1\cos(2t+\phi_{h1}+\phi_{a1}) + aA_1\cos[2(t+\phi_{a1})]\right\}$$
$$+\epsilon^{2+\frac{n_1}{2}}\frac{u_1^{1/2}}{\sqrt{\pi}}\left\{C + \frac{H_1^2}{2}\cos[2(t+\phi_{h1})] + \left(a-\frac{3}{4}\right)A_1H_1\cos(2t+\phi_{h1}+\phi_{a1}) + \left(a-\frac{1}{2}\right)(a-1)\frac{A_1^2}{2}\cos[2(t+\phi_{a1})]\right\}$$
$$+\cdots - Li\epsilon^{2n_1}u_1^2 + \dots\,, \tag{44}$$

with

$$C = \frac{H_1^2}{2} + \left(a-\frac{3}{4}\right)A_1H_1\cos(\phi_{h1}-\phi_{a1}) + \left(a-\frac{1}{2}\right)(a-1)\frac{A_1^2}{2}\,, \tag{45}$$

proportional to the square of the (passive) pitch and heave amplitudes, A_1 and H_1. If $n_1 < 2$, the leading $O(\epsilon^{n_1})$ term of Eq. (44) yields

$$\frac{\partial u_1}{\partial t} = 0\,; \quad \text{i.e.,} \quad u_1 = u_1(\tau)\,, \tag{46}$$

so that the lowest order of u only depends on the slow time τ. On the other hand, in the permanent final state, the leading drag term must balance the leading thrust term. Since the $O(\epsilon^2)$ thrust term only depends on t, the drag term, proportional to u_1^2, must balance the next order in the expansion of $\hat{C}_T$, which contains a constant term; i.e., $2n_1 = 2 + n_1/2$, or $n_1 = 4/3$, which lies between 1 and 2, as assumed. In addition, these terms must balance the leading term on the left-hand side of (44) containing derivatives with the slow time τ; i.e.,

$$b = n_1 = \frac{4}{3}\,. \tag{47}$$

The leading $O(\epsilon^2)$ term of the thrust coefficient must balance the next order on the left-hand side of (44), i.e., $n_2 = 2$, while the following term must be $n_3 = 2n_1 = 8/3$. Thus, the equations at the following two orders, ϵ^2 and $\epsilon^{8/3}$, are

$$R'\frac{\partial u_2}{\partial t} = A_1\left\{H_1\cos(2t+\phi_{h1}+\phi_{a1}) + aA_1\cos[2(t+\phi_{a1})]\right\}, \tag{48}$$

$$R'\left(B\frac{du_1}{d\tau} + \frac{\partial u_3}{\partial t}\right) = \frac{u_1^{1/2}}{\sqrt{\pi}}\left\{C + \frac{H_1^2}{2}\cos[2(t+\phi_{h1})] + \left(a-\frac{3}{4}\right)A_1H_1\cos(2t+\phi_{h1}+\phi_{a1})\right.$$
$$\left. + \left(a-\frac{1}{2}\right)(a-1)\frac{A_1^2}{2}\cos[2(t+\phi_{a1})]\right\} - Liu_1^2\,, \tag{49}$$

respectively. To avoid secular terms in the timescale t, we have the freedom within the two-scales perturbation method [34] to select the equation for $u_1(\tau)$ that cancels the non-oscillatory terms in (49); i.e.,

$$R'B\frac{du_1}{d\tau} = \frac{C}{\sqrt{\pi}}\,u_1^{1/2} - Liu_1^2\,, \tag{50}$$

$$R'\frac{\partial u_3}{\partial t} = \frac{u_1^{1/2}}{\sqrt{\pi}}\left\{\frac{H_1^2}{2}\cos[2(t+\phi_{h1})] + \left(a-\frac{3}{4}\right)A_1H_1\cos(2t+\phi_{h1}+\phi_{a1})\right.$$
$$\left. + \left(a-\frac{1}{2}\right)(a-1)\frac{A_1^2}{2}\cos[2(t+\phi_{a1})]\right\}. \tag{51}$$

Defining

$$u_1(\tau) = U_1 w(\tau)\,, \quad U_1 = \left(\frac{C}{\sqrt{\pi}Li}\right)^{2/3}, \tag{52}$$

and selecting

$$B = \frac{LiU_1}{R'} = \frac{C^{2/3}Li^{1/3}}{\pi^{1/3}R'}\,, \tag{53}$$

with C given by (45), Eq. (50) becomes

$$\frac{dw}{d\tau} = w^{1/2} - w^2\,, \tag{54}$$

so that w always tends to unity as $\tau \to \infty$, and the lowest order (time-averaged) final swimming velocity is

$$U \sim \epsilon^{4/3}\overline{u}_1 = \epsilon^{4/3}U_1\,. \tag{55}$$

The solution of (54) that satifies $w(0) = 0$ can be formally written in implicit form as

$$\tau = 2\frac{w^2 - w^{1/2}}{w^{3/2}-1}F[1, 1/3; 4/3, w^{3/2}]\,, \tag{56}$$

where F is Gauss' hypergeometric function [35].

The oscillatory part of the swimming velocity can be obtained, at the leading orders ϵ^2 and $\epsilon^{8/3}$, from (48) and (51), respectively. Both equations are easily integrated in t, but we shall keep here only the lowest order ϵ^2 from (48), whose solution is

$$u_2 = \frac{A_1}{2R'}\left\{H_1\sin(2t+\phi_{h1}+\phi_{a1}) + aA_1\sin[2(t+\phi_{a1})]\right\} + U_2(\tau)\,, \quad U_2(0) = 0\,. \tag{57}$$

The function $U_2(\tau)$ has to be obtained from the next oder, $\epsilon^{10/3}$, in the same way as done with Eq. (49), but we already have the lowest order dependence of the swimming velocity on τ, $u_1(\tau)$, to which $U_2(\tau)$ is a small correction.

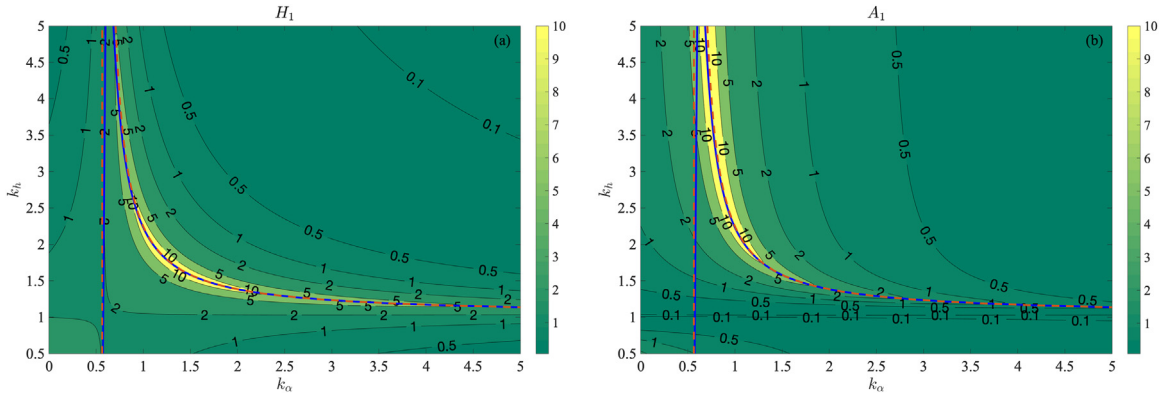

Fig. 2. Contour plots in the $k_\alpha - k_h$ plane of A_1 (a) and H_1 (b) for $a = -1$, $R = 0.02$, $x_0 = 0$, $b_h = b_\alpha = 0.05$. The thick continuous line corresponds to the minimum of $|\det(\mathbf{A})|$, $k_h = k_{hr}(k_\alpha)$, while the dashed one to k_{hr0} given by (41), being the vertical branch $k_{\alpha\infty}$ from (42).

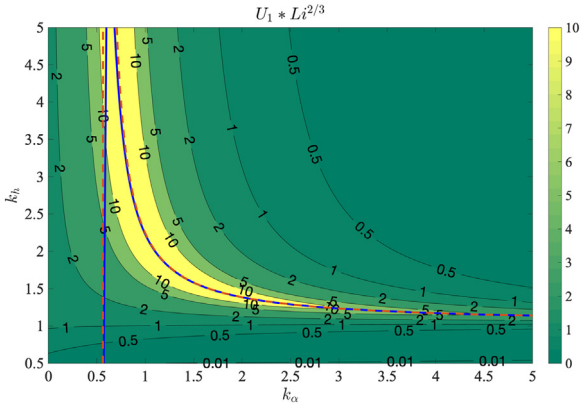

Fig. 3. As in Fig. 2, but for the contours of the scaled lowest order swimming velocity, $ULi^{2/3}/\epsilon^{4/3} \sim U_1 Li^{2/3}$.

5. Self-propulsion characteristics from the lowest order asymptotic solution

Summing up the results of the previous section, the lowest order swimming velocity can be written as

$$u \sim \epsilon^{4/3} U_1 w(\tau) + \epsilon^2 \frac{A_1}{2R'} \left\{ H_1 \sin(2t + \phi_{h1} + \phi_{a1}) + a A_1 \sin[2(t + \phi_{a1})] \right\} + \dots , \quad \tau = \epsilon^{4/3} B t \, , \tag{58}$$

where constants U_1 and B are defined in Eqs. (52) and (53), respectively, and function $w(\tau)$ given by Eq. (56). On the other hand, the lowest order heaving and pitching motions are

$$h = \epsilon H_1 \sin(t + \phi_{h1}) + \dots , \qquad \alpha = \epsilon A_1 \sin(t + \phi_{a1}) + \dots , \tag{59}$$

with H_1, A_1, ϕ_{h1} and ϕ_{a1} given by Eqs. (39)-(40). It is observed that the dimensionless, time-averaged swimming velocity is proportional to $\epsilon^{4/3} U_1 \sim [\epsilon \max(A_1, H_1)]^{4/3}/Li^{2/3}$, i.e., proportional to the pitch or heave amplitude to the power 4/3 divided by the Lighthill number to the 2/3. Thus, to maximize U one has to look for the highest amplitudes of the hydrofoil oscillations and to reduce as much as possible the body drag.

The maxima of A_1 and H_1 are obviously attained at the resonant values of k_h and k_α for given values of the remaining parameters. Actually, these amplitudes become infinity for vanishing dampers constants when $k_h = k_{hr0}$ given by (41) in terms of k_α. Thus, in order to approach the best performance, we shall consider small values of b_h and b_α, just to account for any mechanical friction: $b_h = b_\alpha = 0.05$, say. For these small values, the resonance curve in the $k_\alpha - k_h$ plane at which both A_1 and H_1 reach their maxima is very close to k_{hr0}, as show in Fig. 2 for specific values of the remaining parameters. In particular, we select $R = 0.02$, typical for a hydrofoil in water, a pitch axis at the leading edge ($a = -1$) and the centre of mass coinciding with the centre of the foil ($x_0 = 0$). These values, which are physically justified in §7 below, will be used in all the reported results, except otherwise specified.

As expected, the maxima of the swimming velocity are also reached for $k_h = k_{hr} \simeq k_{hr0}$ as k_α is varied when b_h and b_α are small, as shown in Fig. 3 for the same values of the parameters used in Fig. 2. The quantity $U_1 Li^{2/3} = (C/\sqrt{\pi})^{2/3}$ plotted in this figure is the lowest order swimming velocity scaled with $Li^{2/3}/\epsilon^{4/3}$, which is independent of the Lighthill number and of the torque amplitude ϵ. Clearly, the perturbation solution ceases to be valid as one approaches the resonant curve

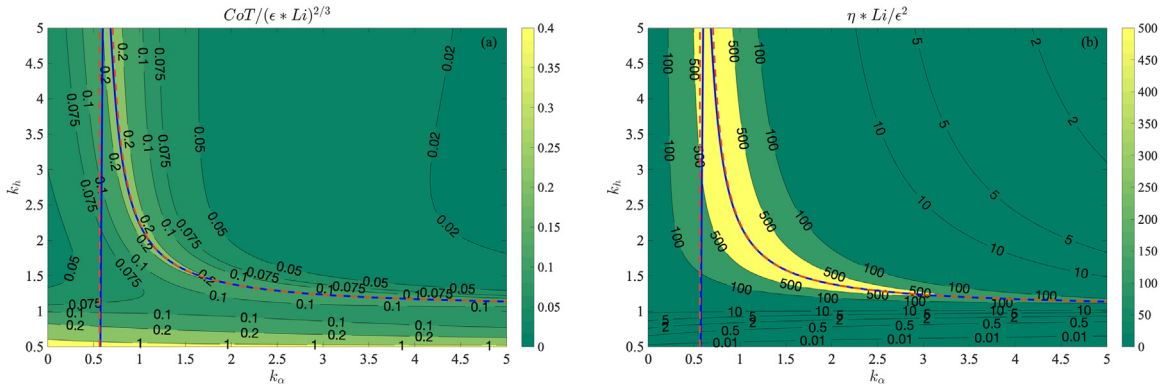

Fig. 4. As in Fig. 2, but for the contours of the scaled lowest order cost of transport, $CoT/(\epsilon Li)^{2/3}$ (a), and the scaled efficiency, $\eta Li/\epsilon^2$ (b).

$k_{hr}(k_\alpha)$ since U_1 becomes so large that the small swimming velocity requirement (32) cannot be satisfied even for very small ϵ. This will be discussed further in Section 6 below, where the lowest order asymptotic solution will be compared with the numerical solution of the model Eqs. (25), (26) and (12), and also with the numerical solutions from the full Navier-Stokes equations in some particular cases.

In addition to the swimming velocity, one is interested in the efficiency and the cost of transport derived from the lowest order asymptotic solution. To that end one has to compute first the power coefficient (17), which, from the above lowest order solution for $\alpha(t)$, is

$$\hat{C}_P \sim \hat{C}_{P1} = -2\epsilon^2 A_1 \cos(t+\phi_{a1}) \sin t\,, \tag{60}$$

and its time average,

$$\overline{\hat{C}}_{P1} = \epsilon^2 A_1 \sin\phi_{a1}\,. \tag{61}$$

With this quantity one may compute the cost of transport (20), which at the lowest order is given by

$$CoT \sim \epsilon^{2/3} \frac{A_1 \sin\phi_{a1}}{U_1} = \frac{\epsilon^{2/3}\pi^{1/3} Li^{2/3} A_1 \sin\phi_{a1}}{C^{2/3}}\,. \tag{62}$$

Finally, the efficiency (18) at this lowest order of the asymptotic solution can be written as

$$\overline{u\hat{C}_T} \sim \epsilon^4 \frac{C}{\sqrt{\pi}} U_1^{3/2} = \epsilon^4 \frac{C^2}{\pi Li}\,, \qquad \eta \sim \epsilon^2 \frac{C^2}{\pi \sin(\phi_{a1}) A_1 Li}\,. \tag{63}$$

Note that the term related to the inertia of the vehicle, proportional to R' in the numerator of (18), does not enter at the lowest order ϵ^4 of the power output $\overline{u\hat{C}_T}$, as already commented on at the end of Section 2. These two alternative efficiencies, CoT and η, are plotted in Fig. 4, scaled in such a way that they are independent of both Li and ϵ, as in the previous figures of this section. The high-efficiency pattern around the resonant values $k_h = k_{hr}(k_\alpha)$ almost coincides with that of the maxima of the swimming velocity, as afore-commented, and with that of local maxima of the cost of transport. This result where the cost of transport behaves inversely to the propulsive efficiency is analogous to that previously found by Akoz and Moored [36] by forcing a constant self-propelled swimming velocity for a defined body via a change of frequency, and in the numerical simulations for a self-propelled fishlike body by Paniccia et al. [18]. Hence, one has to select different values of the spring constants in order to optimize either the Froude efficiency and the swimming velocity or the cost of transport. This will be discussed in more detail below, but using numerical results of the model, not just the present analytical approximation.

Another interesting result is that the Strouhal number (19), which at the lowest order of the asymptotic solution is given by

$$St \sim \frac{2\epsilon[H_1 + (1+|a|)A_1]}{2\pi U} = \frac{Li^{2/3}}{\epsilon^{1/3}} \frac{H_1 + (1+|a|)A_1}{(\pi C)^{2/3}}\,, \tag{64}$$

reaches its minima around the resonant values of $k_h = k_{hr}(k_\alpha)$ (see Fig. 5), where the maxima of η are located.

6. Assessment of the model and numerical results from the model equations

Numerical results of the model equations (25), (26) and (12) with (21), (22) and (27) are presented and discussed in this section. They are solved using Matlab's solver ode45, starting from the initial conditions $\alpha(0) = 0$, $h(0) = 0$ and $u(0) = 0.01$. The results are compared with the lowest order asymptotic solution of the previous Sections 4 and 5. But before that a validation of the model is presented.

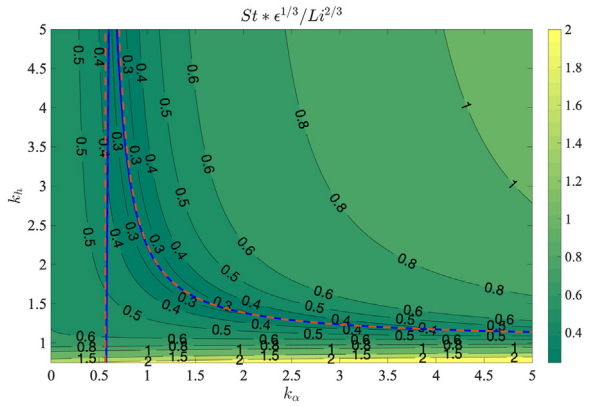

Fig. 5. As in Fig. 2, but for the contours of the scaled lowest order Strouhal number $St\,\epsilon^{1/3}/Li^{2/3}$.

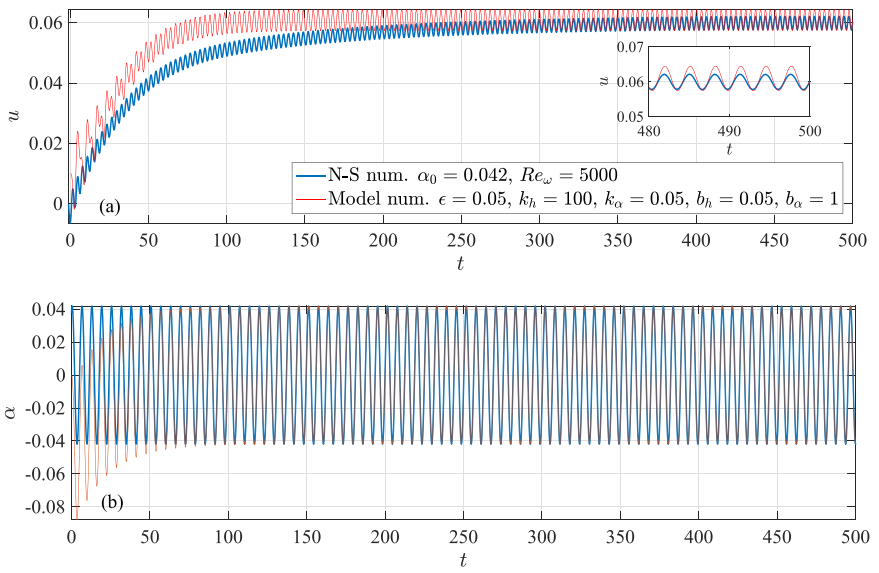

Fig. 6. (a): Comparison between $u(t)$ obtained with $\hat{C}_T$ from full Navier-Stokes numerical simulations (N-S num.) for the pitching motion $\alpha(t) = 0.042\sin t$ given by the blue line in (b), with $u(t)$ from the numerical solution to the model Eqs. (25), (26), (12), (21), (22) and (27) (Model num.) for $\epsilon = 0.05$, $R' = 0.2$, $Li = 0.1$, $R = 0.02$, $a = -1$, $x_0 = 0$, $b_h = 0.05$, $b_\alpha = 1$, $k_h = 100$ and $k_\alpha = 0.05$. (b): $\alpha(t)$ from the model equations generated by the input torque $\hat{C}_{M_i} = \epsilon\sin t$ (red) compared to the input pitch in the N-S simulations (blue). The inset in (a) is a detail of the last cycles of $u(t)$.

As already mentioned in Section 3, the non-stationary thrust force (27) on which the present self-propulsion model is based has already been validated comparing with viscous numerical results and experimental data when the pitching foil is immersed into a uniform current [31], and also with full viscous numerical results of the self-propelled foil for a prescribed pitching motion [13], provided that the pitch amplitude is sufficiently small and the Reynolds number is larger than about 10^3. In relation to this last mentioned work, in the present one the hydrofoil undergoes an additional passive heaving motion generated by Theodorsen's lift force (21) and moment (22), which have been widely validated against experimental data for pitching and heaving rigid foils even for not so small an amplitude of the oscillations when the Reynolds number is large enough [26,27].

Nonetheless, to reinforce this validation for the present problem, that includes a self-propelled vehicle characterized by a drag and a mass through the non-dimensional parameters Li and R', Fig. 6 shows a comparison of the numerical results of the model Eqs. (25), (26), (12), (21), (22) and (27) with those from full viscous numerical simulations for a vehicle with $Li = 0.1$ and $R' = 0.2$ (typical values for a small vehicle with a size of about 1 m, see Section 7 below) self-propelled by a purely pitching foil with pitch amplitude $\alpha_0 = 0.042$ (small enough for the present model be valid). The numerical code, which is fully described and validated in [13], provides the thrust coefficient $\hat{C}_T(t)$ at each instant of time by solving the full Navier-Stokes (N-S) equations for the instantaneous position of the pitching foil, which follows the same dynamical Eq. (12) of the model, but now with $\hat{C}_T(t)$ computed numerically form the exact N-S equations instead of the model (27). In both cases we use for the hydrofoil $R = 0.02$, $a = -1$ and $x_0 = 0$, as in the analytical results reported above. The frequency Reynolds number selected is $Re_\omega = \omega c^2/(4\nu) = 5\,000$, where ν is the fluid kinematic viscosity. The model equations are

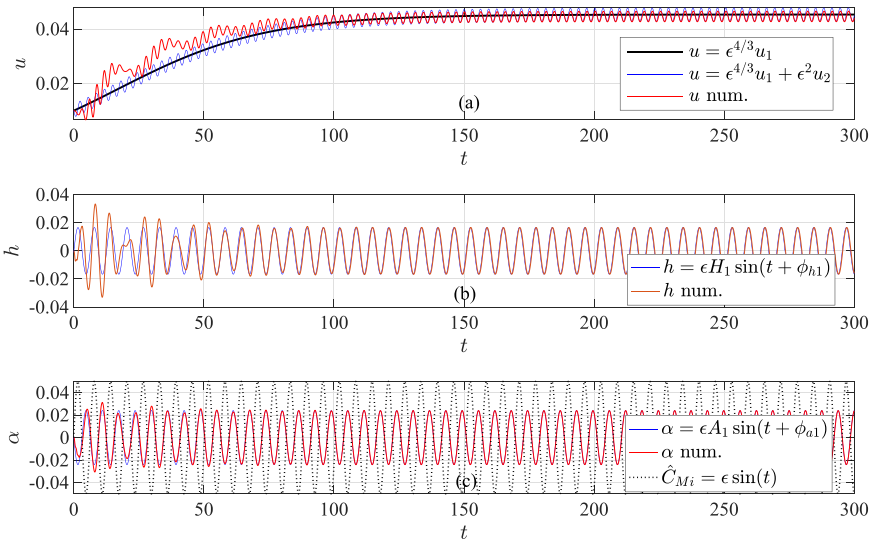

Fig. 7. Comparison between $u(t)$ (a), $h(t)$ (b) and $\alpha(t)$ (c) computed numerically from the model Eqs. (25), (26) and (12) and their analytical lowest order perturbation solutions (58)-(59). The input torque $\hat{C}_{M_i}$ is also included in (c) for reference. $\epsilon = 0.05, R' = 0.2, Li = 0.1, R = 0.02$, $a = -1, x_0 = 0, b_h = b_\alpha = 0.05, k_h = 2.5$ and $k_\alpha = 3$.

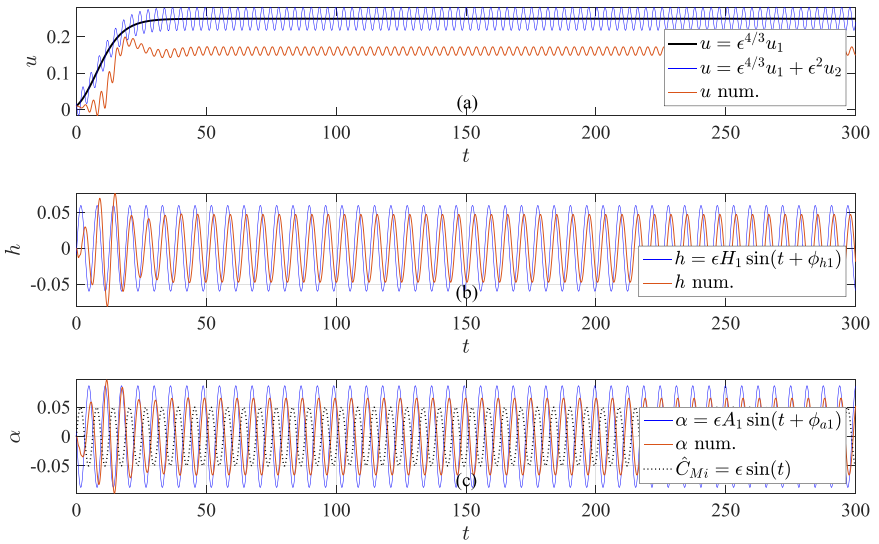

Fig. 8. As in Fig. 7, but for $k_\alpha = 1.5$.

solved with the translational spring constant $k_h = 100$, so that the heaving motion is negligible, thus matching the problem solved numerically for a pure pitching foil, together with $b_h = 0.05$, $k_\alpha = 0.05$ and $b_\alpha = 1$. This last value is selected to reduce as much as possible the transient in $\alpha(t)$ when generated by the torque (1), so that it rapidly approaches the pure pitching motion used as an input in the N-S simulations. As observed in Fig. 6(b), the pitch $\alpha(t)$ from the model equations with torque intensity $\epsilon = 0.05$ rapidly evolves to the value $\alpha = 0.042 \sin t$ used in the N-S simulations. Also note that the corresponding lowest-order pitch amplitude in the asymptotic solution is almost the same, $\epsilon A_1 \simeq 0.044$.

From Fig. 6 it is observed that, despite of the differences in the transient of the pitch $\alpha(t)$, which in the model equations is generated by a sinusoidal torque of given intensity ϵ, instead of being imposed as in the N-S simulations, the numerical results reached for the swimming velocity $u(t)$ from both approaches are very close, yielding almost the same time-averaged swimming speed U and phase, though with larger oscillations when the model is used. Similar results are obtained for other (small) values of α_0 and Re_ω between about 10^3 and 10^4.

Next we compare the analytical asymptotic solution of the previous sections with the numerical solution of the model equations. As mentioned above in §5, the perturbation solution ceases to be valid as the resonant curve $k_{hr}(k_\alpha)$ is approached because U_1 becomes too large (infinite if $b_h = 0$). This is shown in Figs. 7 and 8 for $k_h = 2.5$ when k_α decreases from 3 to 1.5, thus approaching the resonant curve from the right in the $k_\alpha - k_h$ plane (see, e.g., Fig. 2). It is observed that

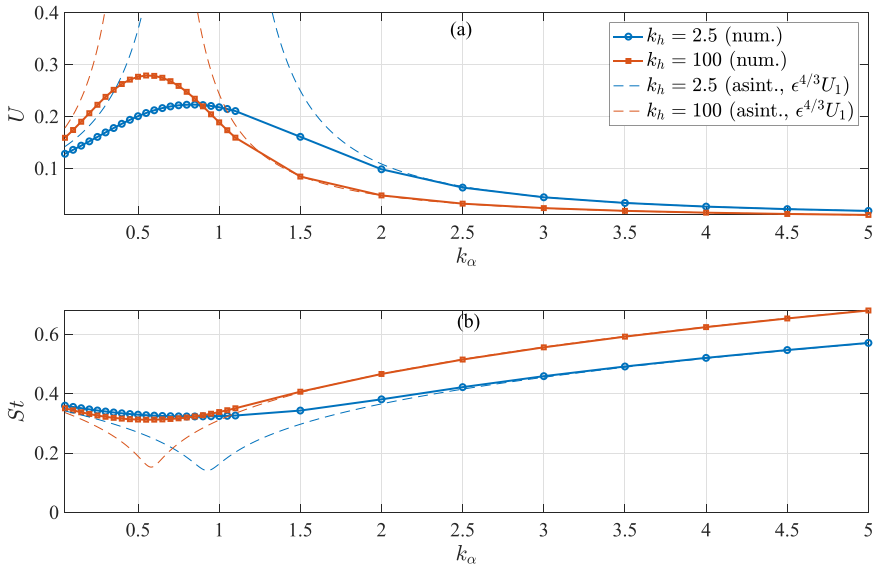

Fig. 9. Comparison between the swimming velocity U (a) and the Strouhal number St (b) computed numerically from the model equations (continuous lines) and their analytical lowest order perturbation solutions (52) and (64) (dashed lines) as a function of k_α for two values of k_h, 2.5 and 100. $\epsilon = 0.05, R' = 0.2, Li = 0.1, R = 0.02, a = -1, x_0 = 0, b_h = b_\alpha = 0.05$.

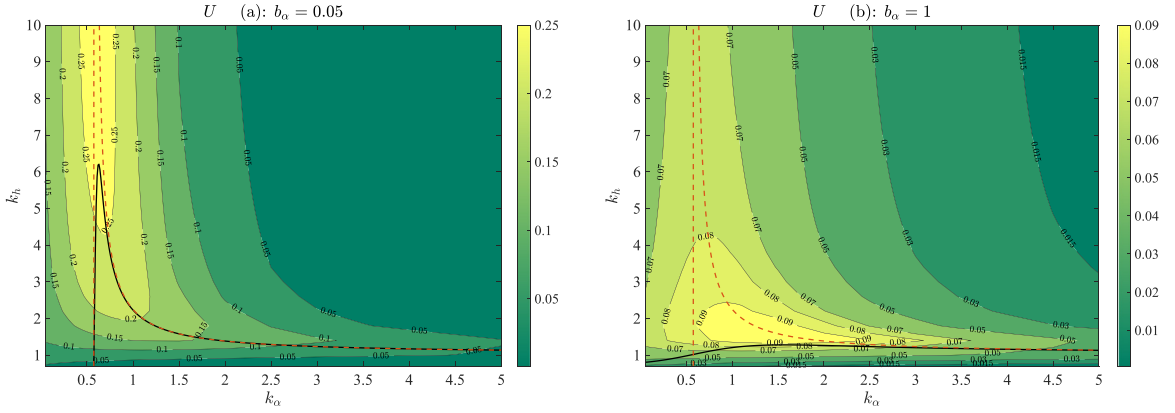

Fig. 10. Contour plots in the $k_\alpha - k_h$ plane of U computed numerically from the model equations (25), (26) and (12) for $b_\alpha = 0.05$ (a) and $b_\alpha = 1$ (b), with $\epsilon = 0.05, R' = 0.2, Li = 0.1, R = 0.02, a = -1, x_0 = 0, b_h = 0.05$. The thick continuous line corresponds to the minimum of $|\det(\mathbf{A})|$, $k_h = k_{hr}(k_\alpha)$, while the dashed one to k_{hr0} given by (41), being the vertical branch $k_{\alpha\infty}$ from (42).

the excellent agreement between the numerical and analytical solutions for $k_\alpha = 3$ in Fig. 7, particularly for the large time oscillatory motion, disappears for $k = 1.5$ in Fig. 8, especially for $u(t)$. This disagreement becomes more pronounced as k_α approaches $k_{hr}(k_\alpha)$ ($\simeq 0.92$ for $k_h = 2.5$), which is better appreciated in Fig. 9. This figure shows the swimming velocity U and the Strouhal number St as k_α is varied for two values of k_h ($k_h = 2.5$ and $k_h = 100$), comparing the numerical solution of the model equations with the lowest order analytical solution. With both approaches, U and St reach their extrema at the corresponding resonant value of k_α for each k_h. Close to this resonance, the perturbation solution ceases to be valid and departs from the numerical one, with peaks (or troughs) much more pronounced than those obtained numerically.

Similarly happens for other values of k_h as k_α is varied. Therefore, the contour plots of the previous Section 5 are reliable except close to the resonant curve, where the extremum values of the different variables are much less pronounced. This can be observed in the left panels of Figs. 10-13, where contour plots in the $k_\alpha - k_h$ plane of U, St, CoT and η, respectively, are plotted for the same small value of the torsional damper constant ($b_\alpha = 0.05$) of Figs. 2-5. As b_α increases ($b_\alpha = 1$ in the right panels of Figs. 10-13), the maxima of U and η (the minima of St and CoT) decrease (increase) and displace towards smaller values of k_h, but always near the corresponding resonant values of k_α, marked with thick lines in Figs. 10, 11, 12, 13. Note that in these figures the different magnitudes are not scaled with ϵ and Li as in the contour plots of the approximate analytical solutions in Figs. 2-5. The torque intensity $\epsilon = 0.05$ and the same typical values of the remaining non-dimensional parameters used in the above comparison with the numerical solution of the full N-S equations have been selected.

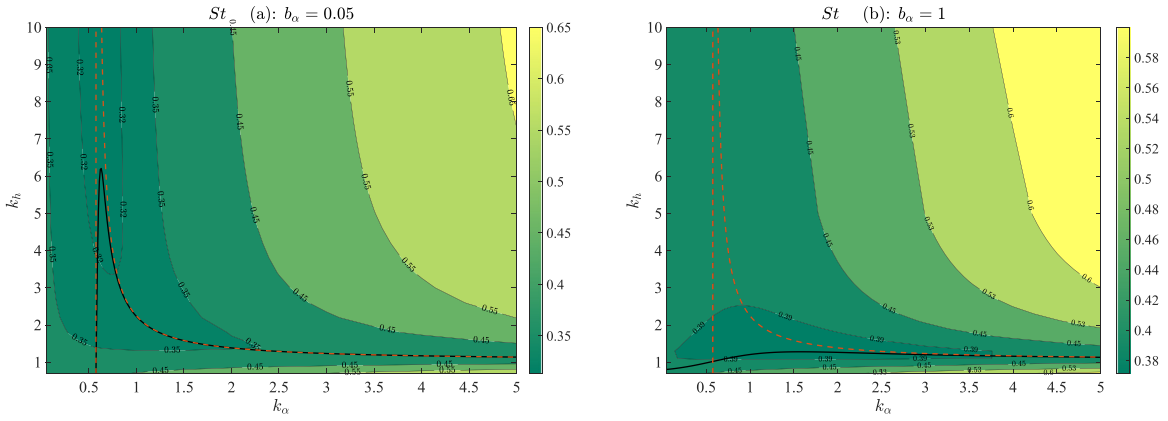

Fig. 11. As in Fig. 10 but for the contours of *St*.

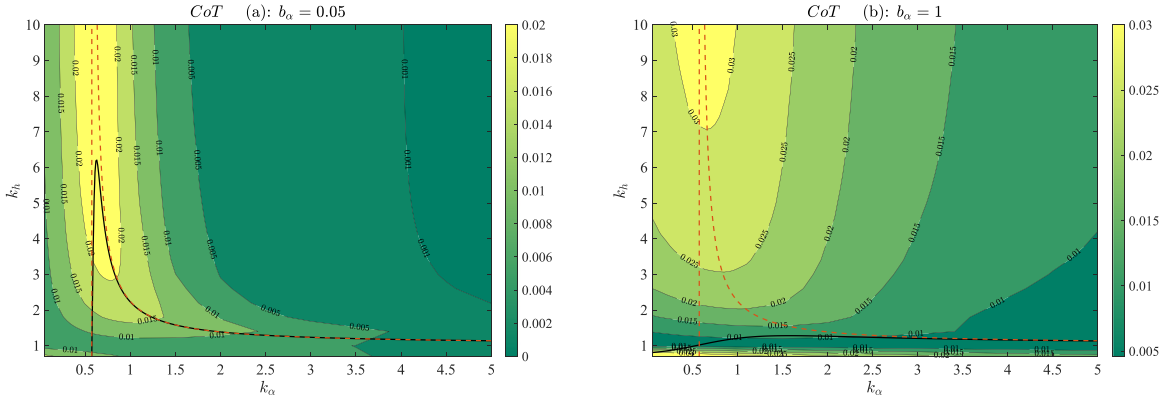

Fig. 12. As in Fig. 10 but for the contours of *CoT*.

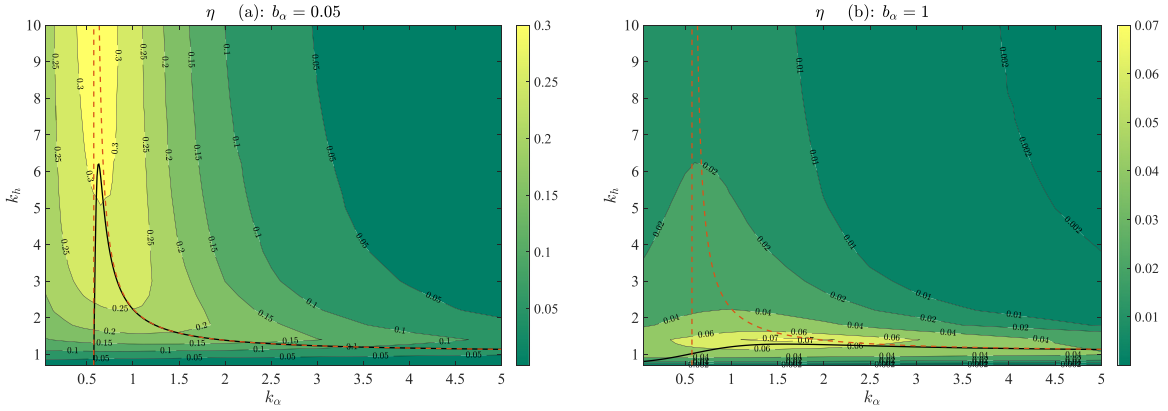

Fig. 13. As in Fig. 10 but for the contours of the efficiency η.

It is noticeable that the maxima of U and η are located close to the values of k_h and k_α where the resonant curve $k_{hr}(k_\alpha)$ has a maximum, decreasing both U and η as the torsional damper constant b_α increases. Thus, the maximum efficiency for $b_\alpha = 0.05$ is almost 35% when $k_\alpha \simeq k_{\alpha\infty} \simeq 0.6$ and $k_h \gtrsim 6$, while, for $b_h = 1$, the maximum η decreases to just above 7% when $k_\alpha \simeq k_h \simeq 1.5$. In the regions with the highest efficiency for each value of b_α, the Strouhal number remains practically constant, below 0.32 for $b_h = 0.05$ and about 0.39 for $b_h = 1$. The first value for the largest efficiency is within the range of Strouhal numbers where many swimming and flying animals in many scales cruise propelled by flapping fins and wings [22,37]. On the other hand, the maxima of *CoT* practically coincide with the maxima of U and η for $b_\alpha = 0.05$, while for $b_h = 1$ the highest values of U and η, which are significantly smaller than for $b_\alpha = 0.05$, are achieved with much lower *CoT*.

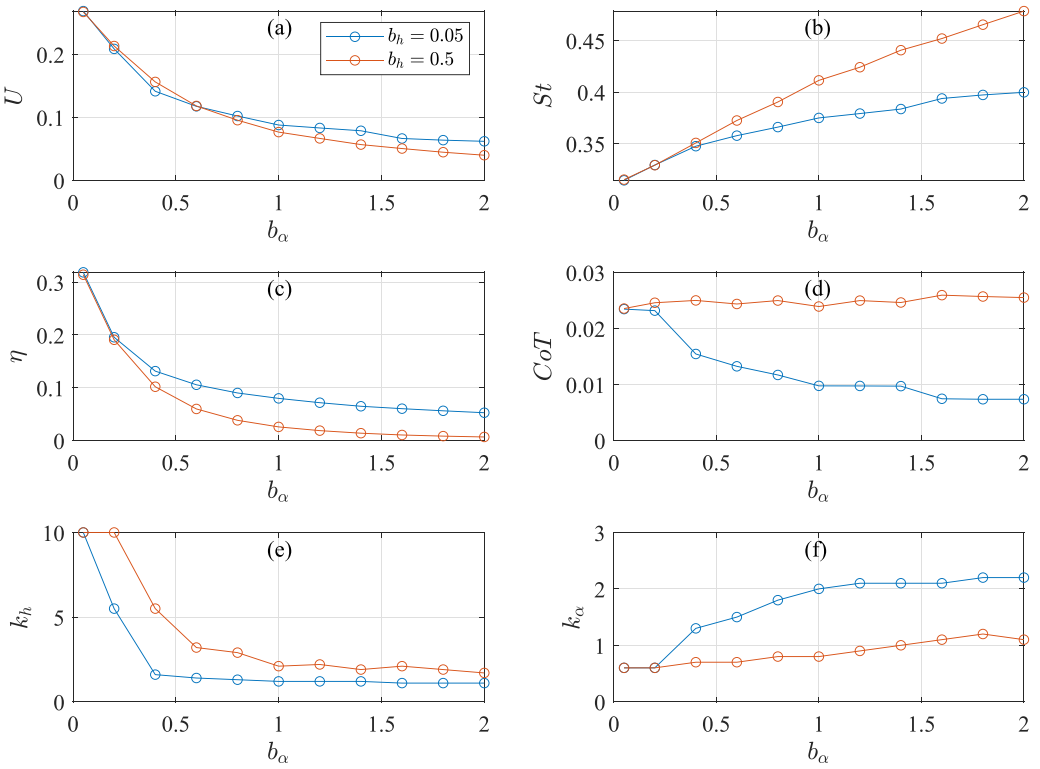

Fig. 14. U (a), St (b), η (c), CoT (d) vs. b_α for two values of b_h (0.05 and 0.5) at the optimal conditions of k_h (e) and k_α (f) where η reaches a maximum value when $0.05 \le k_h \le 10$ and $0.05 \le k_\alpha \le 5$. $\epsilon = 0.05, R' = 0.2, Li = 0.1, R = 0.02, a = -1, x_0 = 0$.

The above contour plots are for a small value of the translational damper constant, $b_h = 0.05$, but the behaviour as b_h increases remains qualitatively the same, only with U and η decreasing slightly, the more so the larger b_α. To better appreciate this, Fig. 14 shows the different magnitudes U, St, CoT and η as functions of b_α for two values of b_h when k_h and k_α are selected to maximize η. The corresponding values of k_h and k_α are also shown. All this for $\epsilon = 0.05, R' = 0.2, Li = 0.1, R = 0.02, a = -1, x_0 = 0$, as in the previous reported results. The figure shows that the maximum value of the efficiency is about 35% as $b_\alpha \to 0$, being almost independent of b_h in this limit. This optimal efficiency is found for the resonant values of the non-dimensional spring constants; particularly, in the range of large k_h (limited to 10 in the optimization process) where $k_\alpha = k_{\alpha\infty}$ given by (42) ($\simeq 0.6$ in the present case). For these conditions, the non-dimensional swimming velocity also reaches its maximum, close to 0.3, and the Strouhal number its minimum about 0.31. However, CoT is about four times larger than its minimal value, which is found to be around 0.007, also for $b_h \to 0$, but now with b_α of order unity or larger, for which the resonant values of k_α (where η reaches its maximum) are larger than $k_{\alpha\infty}$, and k_{hr} is slightly larger than $1 + R$ [see Eq. (41) and, for instance, Fig. 13(b)]. For these conditions, the passive heave amplitude is much larger than the pitch amplitude and both U and η are the smallest. The corresponding Strouhal number is larger, about 0.4.

7. Conclusions

We have developed here a simple model of an aquatic vehicle self propelled by a rigid hydrofoil elastically mounted to translational and torsional springs and dampers that allow for passive heave when the pitching motion is generated by a given sinusoidal torque. The results of the model are obtained by just integrating a set of three ODEs, which are validated with full numerical simulations of the Navier-Stokes equations for sufficiently small pitching amplitudes and frequency Reynolds numbers between about 10^3 and 10^4.

Analytical solutions are also obtained for small non-dimensional swimming velocity, yielding relevant information about the propulsive performance through simple algebraic expressions in terms of the non-dimensional torque amplitude ϵ, the Lighthill number Li, and the remaining dimensionless parameters. Thus, it is found that the non-dimensional swimming velocity behaves as $U \propto \epsilon^{4/3} Li^{-2/3}$ (dimensional swimming velocity $\tilde{U} \propto (M_i/\rho)^{4/3} \omega^{-5/3} c^{-13/3} Li^{-2/3}$, where M_i is the input torque amplitude, ρ the fluid density, c the hydrofoil chord length and ω the forcing angular frequency), the propulsive efficiency as $\eta \propto \epsilon^2 Li^{-1} \propto (M_i/\rho)^2 \omega^{-4} c^{-8} Li^{-1}$, and the dimensionless cost of transport as $CoT \propto (\epsilon\, Li)^{2/3}$ (dimensional cost of transport $\widetilde{CoT} \propto (M_i \omega Li)^{2/3} (\rho c)^{1/3}$). Further, the maxima of the swimming velocity and efficiency are found for the resonant values of the non-dimensional spring constants k_h and k_α, whose expression k_{hr} as a function of k_α and the remaining

non-dimensional parameters is provided with a simple algebraic equation. Particularly, for typical values of the remaining dimensionless parameters (which are discussed below, with a practical example) and dimensionless torque intensity $\epsilon = 0.05$, the highest efficiency found is near 35%, with the highest non-dimensional swimming velocity U close to 0.3, achieved in absence of dampers ($b_h \simeq b_\alpha \simeq 0$) and negligible heaving motion ($k_h \gg 1$) and for the corresponding resonant value of the torsional spring constant, $k_\alpha = k_{\alpha\infty} = [R(a^2 + 1/3) + a^2 + 1/8]/2$, where R is the mass ratio of the foil and a the pivot axis where the torque is applied to the foil. Larger values of ϵ would yield higher values of both η and U as they grow as ϵ^2 and $\epsilon^{4/3}$, respectively, but it has to remain small for the present linear approximation be valid. This configuration with maxima of η and U does not correspond, however, to the minima of CoT, which are also achieved at the resonant values of k_h with negligible translational damper ($b_h \simeq 0$), but now for torsional damper and spring constants larger than unity, corresponding to an almost purely heaving motion, with the resonant value of the translational spring constant k_{hr} slightly larger than $1 + R$. In this limit U and η are close to their minima.

The values of the parameters used in the reported results (other than spring and dampers constants, which are varied in a wide range) are for a typical underwater vehicle (or animal) of a size of the order of the meter with a hydrofoil of chord length about ten times smaller. For instance, for $c = 0.3$ m, $s = 1$ m, $\rho_s = 2\rho$, the selected $R = 0.02$ in water corresponds to a foil thickness $\gamma \simeq 2.4$ mm, which is assumed constant, so that $x_0 = 0$. The pivot axis at the leading edge ($a = -1$) is chosen because it is known to maximize the propulsive performance of a pitching and heaving foil [38]. With these values, the selected $R' = 0.2$ corresponds to a small vehicle's mass of about 14 kg, and $Li = 0.1$ to a vehicle's surface $A_w \simeq 0.094/C_D$ m^2. The value $\epsilon = 0.05$ has been selected small for the model to be valid, but this does not limit the input torque M_i because it is proportional to the square of the flapping frequency according to (1). Thus, with the above foil dimensions in water, the torque amplitude (for $s = 1$ m) is about 6.5 Nm for a frequency $f = 1$ Hz, and about 25 Nm for 2 Hz.

Since the optimal propulsive efficiency and non-dimensional swimming velocity are reached for k_h large, $k_\alpha \simeq k_{\alpha\infty} \simeq 0.6$, and $b_h \simeq b_\alpha \simeq 0$, Eq. (11) gives the dimensional springs and dampers constants once the forcing frequency is selected (note that these expressions are per unit of hydrofoil span). For $f = 1$ Hz, $\tilde{k}_\alpha \simeq 75$ Nm, and 300 Nm for $f = 2$ Hz. Selecting $k_h = 10$, $\tilde{k}_h \simeq 28\,000$ and 112 000 Pa for $f = 1$ and 2 Hz, respectively, while the dampers constants are set to zero, or as low as possible. As aforementioned, the resulting efficiency would be about 35%, for any frequency, and the resulting swimming velocities would be $\tilde{U} \simeq 0.28$ and 0.56 m/s for $f = 1$ and 2 Hz, respectively. Remember that the dimensional velocity increases linearly with f, but at the cost of rapidly increasing the spring constants and the input torque, which are quadratic with f. The dimensional cost of transport would be $\widetilde{CoT} \simeq 10$ and 40 kJ/km for $f = 1$ and 2 Hz, respectively. It may be reduced by a factor of about 4 by selecting $k_h \simeq 1 + R \simeq 1$ and $k_\alpha \simeq 2$, but reducing the swimming velocity and the efficiency more than four times. The corresponding Strouhal number, about 0.4, is larger than that for maximum efficiency, which is about 0.3.

The above results are in qualitative agreement with recent numerical results, both inviscid and viscous, by Paniccia et al. [18] for a fishlike body propelled by an oscillating tail. These authors find also that peak efficiencies are reached for smaller values of the Strouhal number than those where the cost of transport are the lowest, being $\widetilde{CoT}$ higher when η is large, and the efficiency poor when the cost of transport is optimally low. Although the largest efficiencies found by these authors are higher than the present ones because the amplitudes of the tail oscillations in their simulations are not small, like it is assumed the present theory, their reported optimal values of $\widetilde{CoT}$ are quite similar to those found here.

Since the model uses potential flow theory, it cannot be applied to situations where the aquatic vehicle is propelled by large amplitude oscillations of the flapping foil, where flow separation, and particularly the leading edge vortex, plays an important role. In Nature, these situations are usual in fishes for maneuvering and when very high thrust is needed regardless of its efficiency. However, for high efficiency cruising the effective angle of attack of the foil has to be reduced, with weak, or even absence of, vortex formation at the leading edge [38,39]. For these flapping conditions with weak or no flow separation, for which the present theoretical model is intended, the lift and thrust forces given by the potential flow theory agree quite well with experimental data of pitching and heaving foils, surprisingly even for not so small amplitude of the oscillations [26,27,29,31]. The present results, especially the numerical results of the model equations which are not as limited in amplitude as the analytical asymptotic results, would be applicable for modeling the efficient cruising of real aquatic vehicles propelled by a biomimetic flapping foil. This is supported by the fact that the Strouhal numbers found for the optimal efficiency conditions at resonance are always within the range where many swimming and flying animals, of many scales, cruise propelled by flapping fins and wings [22,37].

Data availability

Data will be made available on request.

Acknowledgments

This research has been supported by the Junta de Andalucía, Spain, through the project grants UMA18-FEDER-JA-047 and P18-FR-1532. The computations were performed in the Picasso Supercomputer at the University of Málaga, a node of the Spanish Supercomputing Network. Funding for open access charge: Universidad de Málaga / CBUA.

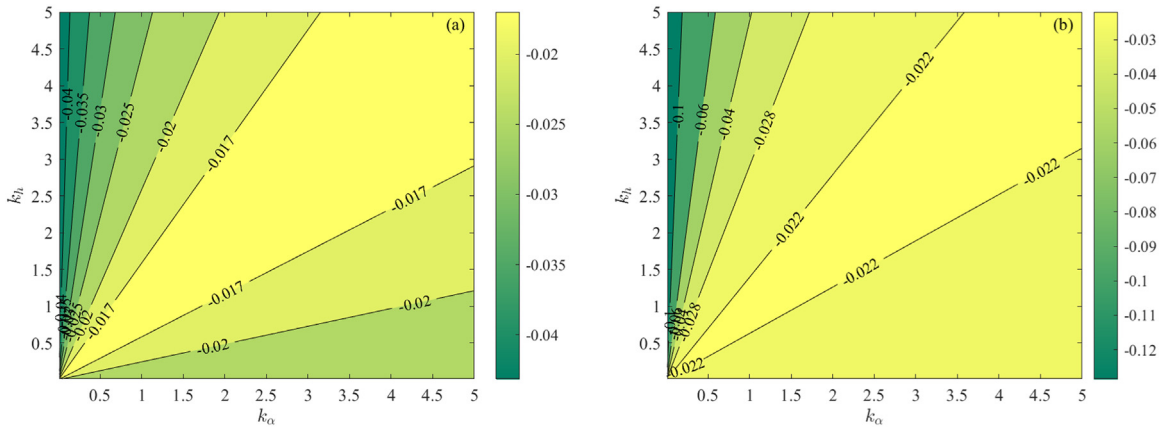

Fig. A1. Contour plots in the $k_\alpha - k_h$ plane of max[Re(λ_1)] for $R = 0.02$, $x_0 = 0$, $b_h = b_\alpha = 0.05$, and for $a = -1$ (a) and $a = -0.5$ (b).

Appendix A. Eigenvalues of Eq. (37)

Without dampers, $b_h = b_\alpha = 0$, and for $x_0 = 0$, the solution of (37) has no real part,

$$\lambda_1 = \pm i\left(\frac{2k_\alpha(R+1) + k_h(RI_a + a^2 + 1/8)}{R^2/3 + 11R/24 + 1/8}\right)^{1/2}, \tag{A.1}$$

and the system is always neutrally stable. For $x_0 = 0$ and any positive values of the dampers constants b_h and b_α, Re(λ_1) is found to be negative, and therefore the system stable, for any value of k_h and of k_α, and for all physically relevant values of R and a which have been considered. As an example, Fig. A.1 shows the results in the plane (k_α, k_h) of the maximum of Re(λ_1) for $b_h = b_\alpha = 0.05$, $R = 0.02$ and two values of a. Similar results are found for $-1 \le a \le x_0 = 0$ (i.e., pitching axis upstream of the center foil, which is the center of mass) and any value of R. Actually, the system becomes more stable as R increases.

References

[1] K.V. Rozhdestvensky, V.A. Ryzov, Aerohydrodynamics of flapping-wing propulsors, Prog. Aero. Sci. 39 (2003) 585–633.
[2] M. Platzer, K. Jones, J. Young, J. Lai, Flapping wing aerodynamics: progress and challenges, AIAA J. 46 (2008) 2136–2149.
[3] B. Augier, J. Yan, A. Korobenko, J. Czarnowski, G. Ketterman, Y. Bazilevs, Experimental and numerical FSI study of compliant hydrofoils, Comput. Mech. 55 (2015) 1079–1090.
[4] X. Wu, X. Zhang, X. Tian, X. Li, W. Lu, A review on fluid dynamics of flapping foils, Ocean Eng. 195 (2020) 106712.
[5] M.M. Murray, L.E. Howle, Spring stiffness influence on an oscillating propulsor, J. Fluids Structures 17 (2003) 915–926.
[6] A.W. Mackowski, C.H.K. Williamson, Effect of pivot point location and passive heave on propulsion from a pitching airfoil, Phys. Rev. Fluids 2 (2017) 013101.
[7] R. Fernandez-Feria, J. Alaminos-Quesada, Energy harvesting and propulsion of pitching airfoils with passive heave and deformation, AIAA J. 60 (2) (2022) 783–797.
[8] Q. Zhu, Z. Peng, Mode coupling and flow energy harvesting by a flapping foil, Phys. Fluids 21 (2009) 033601.
[9] Q. Zhu, M. Haase, C.H. Wu, Modeling the capacity of a novel flow-energy harvester, Appl. Math. Model. 130 (2009) 2207–2217.
[10] J. Deng, L. Teng, D. Pan, X. Shao, Inertial effects of the semi-passive flapping foil on its energy extraction efficiency, Phys. Fluids 27 (2015) 053103.
[11] Y. Su, K. Breuer, Resonant response and optimal energy harvesting of an elastically mounted pitching and heaving hydrofoil, Phys. Rev. Fluids 4 (2019) 064701.
[12] P. Ma, G. Liu, Y. Wang, Y. Zhang, Y. Xie, Numerical study on the hydrodynamic performance of a semi-passive oscillating hydrofoil, Ocean Eng. 223 (2021) 108649.
[13] R. Fernandez-Feria, E. Sanmiguel-Rojas, P.E. Lopez-Tello, Numerical validation of simple non-stationary models for self-propelled pitching foils, Ocean Eng. 260 (2022) 111973.
[14] S. Alben, M. Shelley, Coherent locomotion as an attracting state for a free flapping body, Proc. Nat. Acad. Sci. USA 102 (32) (2005) 11163–11166.
[15] J. Sánchez-Rodríguez, C. Raufaste, M. Argentina, A minimal model of self propelled locomotion, J. Fluids Structures 97 (2020) 103071.
[16] X. Lin, J. Wu, T. Zhang, Self-directed propulsion of an unconstrained flapping swimmer at low Reynolds number: hydrodynamic behaviour and scaling laws, J. Fluid Mech. 907 (2021) R3.
[17] L.B. Ramos, O. Marquet, M. Bergmann, A. Iollo, Fluid-solid Floquet stability analysis of self-propelled heaving foils, J. Fluid Mech. 910 (2021) A28.
[18] D. Paniccia, L. Padovani, G. Graziani, R. Piva, The performance of a flapping foil for a self-propelled fishlike body, Sci. Rep. 11 (2021) 22297.
[19] T. Theodorsen, General theory of aerodynamic instability and the mechanism of flutter, 1935, Tech. Rep. TR 496, NACA.
[20] M. Gazzola, M. Argentina, L. Mahadevan, Scaling macroscopic aquatic locomotion, Nat. Phys. 10 (2014) 758–761.
[21] D. Gross, Y. Roux, C. Raufaste, M. Argentina, Drag analysis with a self-propelled flexible swimmer, Phys. Rev. Fluids 6 (2021) 053101.
[22] G.S. Triantafyllou, M.S. Triantafyllou, M.A. Grosenbaugh, Optimal thrust development in oscillating foils with application to fish propulsion, J. Fluid Structures 7 (1993) 205–224.
[23] A. Das, R.K. Shukla, R.N. Govardhan, Contrasting thrust generation mechanics and energetics of flapping foil locomotory states characterized by a unified St-Re scaling, J. Fluid Mech. 930 (2022) A27.
[24] G. Gabrielli, T. von Kármán, What price speed? Specific power required for propulsion, J. Am. Soc. Naval Eng. 63 (1951) 188–200.
[25] J.M. Greenberg, Airfoil in sinusoidal motion in a pulsating stream, 1947, Tech. Rep. TR 1326, NACA.
[26] R.L. Halfman, Experimental aerodynamic derivatives of a sinusoidally oscillating airfoil in two-dimensional flow, 1952, Tech. Rep. TR 1108, NACA.

[27] Y.S. Baik, L.P. Bernal, K. Granlund, M.V. Ol, Unsteady force generation and vortex dynamics of pitching and plunging aerofoils, J. Fluid Mech. 709 (2012) 37–68.
[28] R. Fernandez-Feria, Linearized propulsion theory of flapping airfoils revisited, Phys. Rev. Fluids 1 (2016) 084502.
[29] R. Fernandez-Feria, Note on optimum propulsion of heaving and pitching airfoils from linear potential theory, J. Fluid Mech. 826 (2017) 781–796.
[30] R. Fernandez-Feria, E. Sanmiguel-Rojas, Comparison of aerodynamic models for two-dimensional pitching foils with experimental data, Phys. Fluids 31 (2019) 057104.
[31] J. Alaminos-Quesada, Limit of the two-dimensional linear potential theories on the propulsion of a flapping airfoil in forward flight in terms of the Reynolds and Strouhal number, Phys. Rev. Fluids 6 (12) (2021) 123101.
[32] R. Fernandez-Feria, J. Alaminos-Quesada, Propulsion and energy harvesting performances of a flexible thin airfoil undergoing forced heaving motion with passive pitching and deformation of small amplitude, J. Fluids Structures 102 (2021) 103255.
[33] I.E. Garrick, Propulsion of a flapping and oscillating airfoil, 1936, Tech. Rep. TR 567, NACA.
[34] J. Kevorkian, J.D. Cole, Perturbation methods in applied mathematics, Springer-Verlag, New York, 1981.
[35] F.W.J. Olver, D.W. Lozier, R.F. Boisvert, C.W. Clark (Eds.), NIST Handbook of Mathematical Functions, Cambridge University Press, Cambridge (UK), 2010.
[36] E. Akoz, K.W. Moored, Unsteady propulsion by an intermittent swimming gait, J. Fluid Mech. 834 (2018) 149–172.
[37] G.K. Taylor, R.L. Nudds, A.L.R. Thomas, Flying and swimming animals cruise at a Strouhal number tuned for high power efficiency, Nature 425 (2003) 707–711.
[38] I.H. Tuncer, M. Kaya, Optimization of flapping airfoils for maximum thrust and propulsive efficiency, AIAA J. 43 (2005) 2329–2336.
[39] J.M. Anderson, K. Streitlien, K.S. Barret, M.S. Triantafyllou, Oscillating foils of high propulsive efficiency, J. Fluid Mech. 360 (1998) 41–72.